

Article

A Numerical Feasibility Study of Kinetic Energy Harvesting from Lower Limb Prosthetics

Yu Jia ^{1,2,*}, Xueyong Wei ³, Jie Pu ², Pengheng Xie ², Tao Wen ², Congsi Wang ⁴, Peiyuan Lian ⁴, Song Xue ⁴ and Yu Shi ^{2,*}

¹ School of Engineering and Applied Science, Aston University, Birmingham B4 7ET, UK

² Department of Mechanical Engineering, University of Chester, Chester CH2 4NU, UK; 1821721@chester.ac.uk (J.P.); 1821700@chester.ac.uk (P.X.); t.wen@chester.ac.uk (T.W.)

³ State Key Laboratory for Manufacturing Systems Engineering, Xian Jiaotong University, 28 West Xianning Road, Xi'an 710049, China; seanwei@mail.xjtu.edu.cn

⁴ Key Laboratory of Electronic Equipment Structure Design, Xidian University, Xi'an 710071, China; congsiwang@163.com (C.W.); lian100fen@126.com (P.L.); sxue@xidian.edu.cn (S.X.)

* Correspondence: yu.jia.gb@ieee.org (Y.J.); y.shi@chester.ac.uk (Y.S.)

Received: 9 August 2019; Accepted: 6 October 2019; Published: 10 October 2019



Abstract: With the advancement trend of lower limb prosthetics headed towards bionics (active ankle and knee) and smart prosthetics (gait and condition monitoring), there is an increasing integration of various sensors (micro-electromechanical system (MEMS) accelerometers, gyroscopes, magnetometers, strain gauges, pressure sensors, etc.), microcontrollers and wireless systems, and power drives including motors and actuators. All of these active elements require electrical power. However, inclusion of a heavy and bulky battery risks to undo the lightweight advancements achieved by the strong and flexible composite materials in the past decades. Kinetic energy harvesting holds the promise to recharge a small on-board battery in order to sustain the active systems without sacrificing weight and size. However, careful design is required in order not to over-burden the user from parasitic effects. This paper presents a feasibility study using measured gait data and numerical simulation in order to predict the available recoverable power. The numerical simulations suggest that, depending on the axis, up to 10s mW average electrical power is recoverable for a walking gait and up to 100s mW average electrical power is achievable during a running gait. This takes into account parasitic losses and only capturing a fraction of the gait cycle to not adversely burden the user. The predicted recoverable power levels are ample to self-sustain wireless communication and smart sensing functionalities to support smart prosthetics, as well as extend the battery life for active actuators in bionic systems. The results here serve as a theoretical foundation to design and develop towards regenerative smart bionic prosthetics.

Keywords: human motion; prosthetics; energy recovery; gait; smart devices

1. Introduction

Lower limb prosthetics are crucial to the quality of life of amputees, by making it possible to lead both an independent and physically active lifestyle [1]. One of the earliest documented examples of lower limb prosthetics date back to the Romans, circa 300 B.C. [2], along with mentions of the use of artificial limbs within the Graeco-Roman literature. An early contemporary iteration dates back to the 1950s with the invention of the SACH (solid ankle cushion heel) foot [3], followed by various other embodiments in

the ensuing decades such as the Flex foot with its blade spring designs primarily for sports and the Seattle foot with more efficient energy absorbing metal springs and foams acting as dampers [4].

Development of prosthetics since the 1980s also involved the increasing use of composite materials such as carbon fibre [5], as a lightweight, flexible and strong material compared with plastic, wood and metal. The lightweight composite structure brings comfort for users while also offering a better mechanical robustness when interacting with the environment. The advent and adoption of energy storage and return (ESR) prosthetics, which contains a mechanical spring or pneumatic restoring force mechanism, can help to minimise user's energy expenditure compared to traditional solid prosthetics [6]. More recently, there is a growing research interest to include active elements, such as active ankle and knee driven by actuators and controlled by feedback information from sensors, to develop towards lower limb bionics in order to further reduce the human energy cost and improve gait pattern of transtibial amputees [7]. A key conceptual measure of merit adopted by many academic and industrial researchers is the 3Cs: control, comfort and cosmetics [8]. An ideal prosthetics is thought to possess a high 3C-level.

Some of the key advances in contemporary lower limb prosthetics, including their working mechanisms, merits and challenges, are summarised below and in Figure 1,

- *Conventional Solid Cushioned Prosthetics:* They are typically made of solid wood, plastic or metal structures, with some soft cushioning with foam or rubber to provide a degree of comfort and energy efficiency. The basic principle is not too distinct from solid prosthetics reported since antiquity. A key design feature is to mimic human leg and feet from a cosmetic point of view. The primary aim is to enable basic gait functionality to an amputee. However, the non-optimised gait pattern from these prostheses can stress the healthy limbs and joints, causing injury after prolonged use. A classical example is the SACH foot, which has an energy efficiency estimated up to 31% [9]. Users are required to manually control these solid prosthetics, and this is typically described as passive control. The gait is typically unnatural with limping patterns, which can result in repeated stress injuries to other health body parts such as joints, limbs and hip.
- *Energy Storage and Return (ESR):* They typically contain a spring component acting as a restoring force mechanism, allowing mechanical energy to be momentarily stored and returned to the gait motion while walking and running. The spring can either be a linear mechanical spring or a second-order pneumatic air spring. The use of ESR in prosthetics design since the 1980s has been considered as a crucial milestone towards helping to improve gait pattern and behaviour based on biomechanics research [5]. The ESR mechanism can generally be modelled as a second-order mass–spring–damper system, with a focus on the restoring force term.

Key optimisation parameters include minimising damping and synchronising energy return rate to the gait speed. When a runner's rate of compression of the ESR prosthetics is close to the resonant frequency of the ESR foot, energy efficiency can be maximised. Classic examples include the Flex foot mainly used in sports and the Seattle foot that incorporates springs into a cushioned foot. The springs themselves can either be mechanical spring structures made of metal, plastic or composite materials, or pneumatic springs relying on air or fluidic pressure as the restoring force. Seattle and Flex come in various design embodiments, with energy efficiency estimated up to 52% and 84%, respectively [9].

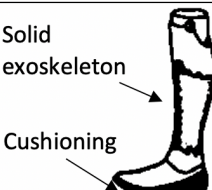
- *Composite Materials:* The use of carbon fibre reinforced polymer (CFRP) composites coincided with the development of the Flex foot and Seattle foot, primarily as part of the employed spring material within the lower limb [10] in contrast to metallic springs due to CFRP's lightweight, flexibility and high strength [5]. CFRP can be five times lighter than steel while offering either similar or up to an order of magnitude higher tensile strength. This is seen in both as a critical enabling material for professional sports as well as a high performance material in commercial prosthetics.

Amputee athletes with CFRP c-shaped flexible lower limb prosthetics are able to attain athletic records that are just about 10% lower than abled-bodied athletic records [5]. Furthermore, in commercial prosthetics, the use of CFRP and ESR prosthetics have been crucial to reduce stress on the joints and hips of the amputees compared to conventional solid cushioned prosthetics [11]. Composite materials are also possible to be integrated with functional materials such as piezoelectric transducers to enable sensing and harvesting capabilities [12].

- *Bionics and Active Control:* While ESR prosthetics provide a better energy efficiency and comfort than traditional solid cushioned prosthetics, gait behaviour is still far from ideal [7]. Improper gait can result in repeated stress and injury to the healthy parts of the human body. More recently, there has been an increasing trend in prosthetics research to develop towards bionics leg and feet, where motors and actuators [13] integrated with active or semi-active control systems [14] are used to control the motion of ankles and knees. The aim is to mimic the natural human biomechanics and gait pattern, where gait information gathered from sensors are used to control the knee and ankle orientations in order to improve towards the biomechanics of a normal gait [15].

The active or semi-active control of these bionic prosthetics involve various integrated sensors along with variable damping, actuation power drive and artificial intelligence [16]. However, some of the design challenges include aiming to achieve high force/torque and power efficiency while minimising weight and size of the drive and power systems [17]. In particular, the weight of the batteries to power the sensors and drive systems can be a key limiting factor while trying to optimise between operation time and weight.

A study that assumed a basic system using two motors to control knee and ankle has estimated that a lithium polymer battery pack of reasonable size and weight can attain a range of 5 km [18]. The goal is to extend this range to maximise mobility and life quality for amputees. However, to have full degrees of freedom in control, motor actuators are required on all three axes for both knee and ankle, thus requiring even more power and limiting the practical range further. Fortunately, the motors and actuators used to control prosthetic knee and ankle are not required to continuously operate in active mode and many semi-active strategies have been proposed [19]. The active operation time period of servo motors can be as short as 10 ms to make a minute and precise angular orientation correction. Most of the time, these motors can be put into sleep mode in order to conserve energy. The use of energy harvesting can potentially help to recharge the on-board battery and compensate the intermittent energy drains by the motors.

 Pre-1980s	 1980s onwards	 Now and future
Solid exoskeleton Cushioning	Pneumatic spring and force sensors	Composite body and springs Spring restoring designs Active knee Sensors, wireless, controllers Active spring control Active knee

Solid prosthetics with soft cushioning. High cosmetics, low control and low comfort.	Energy storage and return for high energy efficiency. Moderate cosmetics, low control and moderate comfort.	Composite materials for lightweight, strength and flexibility. Moderate cosmetics, moderate control and moderate comfort	Bionics composite prosthetics, with smart gait and condition monitoring. High cosmetics, high control and high comfort.
--	---	--	---

Figure 1. Brief summary of the evolution of lower limb prosthetics through the ages.

Coupled with bionics, there is also a trend towards smart devices and materials aimed at enabling gait and condition monitoring. Some of the sensors integrated for gait and condition monitoring include MEMS (microelectromechanical systems) accelerometers, gyroscopes, magnetometers, strain gauges and pressure gauges. These sensors and the power actuators for bionics are all controlled by microcontrollers and wireless communication systems. This implies that there is an increasing number of active components on the prosthetics that require electrical power, which in turn places a heavier burden on battery requirements.

Depending on the mass distribution, there can be a non-trivial amount of kinetic energy experienced and dissipated during the prosthetic gait [20]. By harvesting some of the kinetic energy during gait and converting it into electrical energy, the power requirements of the sensors and drive systems of a smart and/or bionic prosthetics can be supplemented. This regenerative energy approach is particularly useful to continuously recharge a given small battery source, in order to minimise weight of the prosthetics.

Mechanical power can be converted into useful electrical power to enable a self-sustaining power source for the sensors and actuators/motors. Transducers, such as electromagnetic [21,22], piezoelectric [23,24], electrostatic [25,26] and triboelectric [27,28] transducers, are some of the more popular mechanical-to-electrical energy conversion methods [29]. These transducers can either be parasitically attached to the main springs within the prosthetics, or entirely replace the main springs.

However, careful power control and damping switching are required to prevent over-burdening the user with unnecessary parasitic effects [30,31]. The idea is to recover kinetic energy which would otherwise be dissipated to the ambience, and not drawing extra energy from the user. It has been identified that such an energy window does exist within the biomechanics of prosthetic gait during the restoring cycle of sprung elements, in what is described as the limb's regenerative region of operation [32].

Therefore, switch-based [33] control power electronics is required to only harvest kinetic energy during this part of the gait cycle. By controlling the electrical damping of these transducers, it is also possible to enable active control and only extract energy during the unintrusive time windows, while acting as a purely restoring spring during other time windows in order to assist gait motion and comfort.

This paper uses measured acceleration data from various gait patterns to numerically simulate the recoverable power from a potential regenerative prosthetics. This is compared against typical sensor, microprocessor unit and actuator power requirements in order to assess the feasibility of using kinetic energy harvesting from lower limb prosthetics to minimise the on-board battery size.

2. Method

2.1. Gait Measurement and Analysis

Pedometry acceleration data were measured from a healthy able-bodied 34 years old male with body mass of 70 kg from various gait conditions. Ideal bionic prosthetics enabled amputee is theorised to be able to walk in a similar fashion. A three-axis accelerometer data logger was placed at the right foot of the participant, inside the sneaker. The three axes of the accelerometer data shown in this paper correspond to the following axes of the human body:

- Accelerometer x axis (1): sagittal axis
- Accelerometer y axis (2): longitudinal axis
- Accelerometer z axis (3): frontal axis

The measurements were taken at a sampling rate of 800 Hz. However, typically, gait frequency features can usually be captured within the first 10 Hz. Therefore, the sensor resolution was more than sufficient to provide accurate reconstruction of the gait motion in all three axes. The following types of gait conditions were captured:

- Walking at 3 km/h
- Walking at 6 km/h
- Running at 9 km/h
- Climbing at 30 steps per minute
- Climbing at 40 steps per minute
- Climbing at 60 steps per minute
- Walking at 3 km/h with 20 kg weight in the left hand to simulate limping
- Walking at 3 km/h with 20 kg weight in the right hand to simulate limping

The step length, as set by the step treadmill and the standard flat treadmill, averages around 70 cm. The step height ranges between 10 and 20 cm depending on the stride speeds defined by the step rate and walking speeds of the treadmills. Gait parameters for the measurements taken were relatively uniform for a particular gait condition. The key data to be extracted here were the three-axis acceleration measurement from each gait type and condition, controlled by the various treadmills and speed settings.

2.2. Analytical and Numerical Model

The mechanics of the lower limb prosthetics assumed in this study is that of a combined pneumatic air spring on a mechanical composite spring, which is a common state-of-the-art ESR composite prosthetic design [17]. The analytical equations of force and motion were derived to mathematically describe the dynamics of the prosthetics while subjected to external acceleration loading while walking and running. The measured gait acceleration data can then be numerically computed into the model in order to predict the response from the system, including response displacement, velocity, acceleration, kinetic energy and potential recoverable electrical energy information.

The analytical model was numerically computed in MATLAB using the measured acceleration gait data in order to predict the recoverable power. ODE45 solver was used to numerically compute the analytical equations given in Section 3.1 in order to estimate the time domain response and recoverable power. Measured acceleration traces were pre-processed and condition as the input signal to feed into the numerical model. An overview of the measurement and simulation method is summarised in Figure 2.

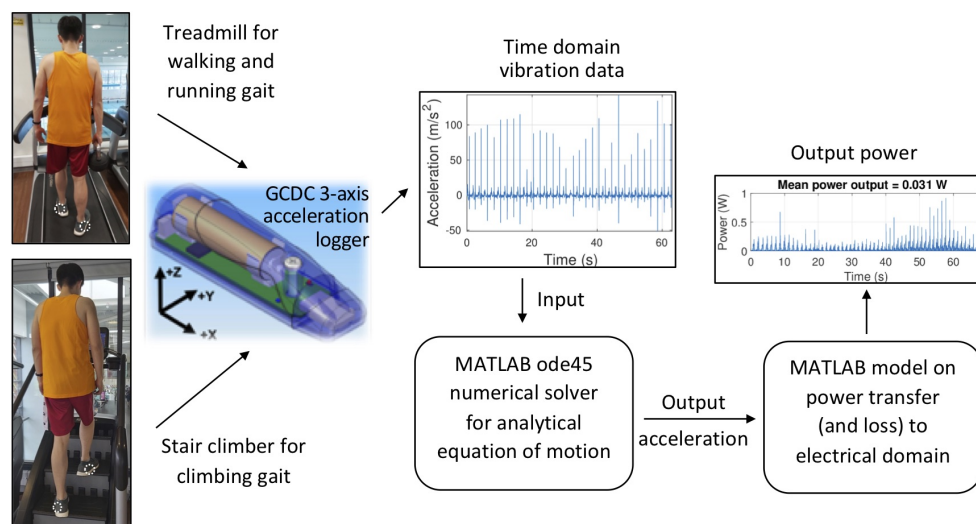


Figure 2. Overview of measurement and numerical simulation method. White dotted circles illustrate the location of the accelerometers, which are fixed on the inside of the shoes.

A factor 0.1 is applied to all simulated power values shown in the plots to account for 50% transduction loss [34], followed by 20% power conditioning loss and a simultaneous 20% electrical parasitic loss [35], and finally only harvesting one third of the gait kinetic energy ($(1 \times 0.5 \times 0.6) \div 3 = 0.1$).

3. Results

3.1. Analytical and Finite Element Model

This paper focuses on a typical modern ESR lower limb prosthetic design illustrated in Figure 3 [36], with a pneumatic air spring below the knee and a carbon fibre mechanical spring as the foot. The first resonant frequency of the prosthetics is simulated using finite element analysis as shown in the figure, assuming an above-limb total body mass of 70 kg (35 kg on each lower limb). It can be seen that the eigenfrequency solver revealed the first resonant frequency to be around 2.8 Hz, implying an ideal energy efficiency while running near this frequency of footfall, which is near the typical strides per second for a typical athletic running gait of 3 Hz [37]. However, most average non-athletic human running gait is unlikely to exceed a sustained stride rate of 2 Hz. The resonant build up of the prosthetics spring mechanism helps to more efficiently execute the energy storage and return function, but such an operation is potentially unsafe for untrained non-athletes.

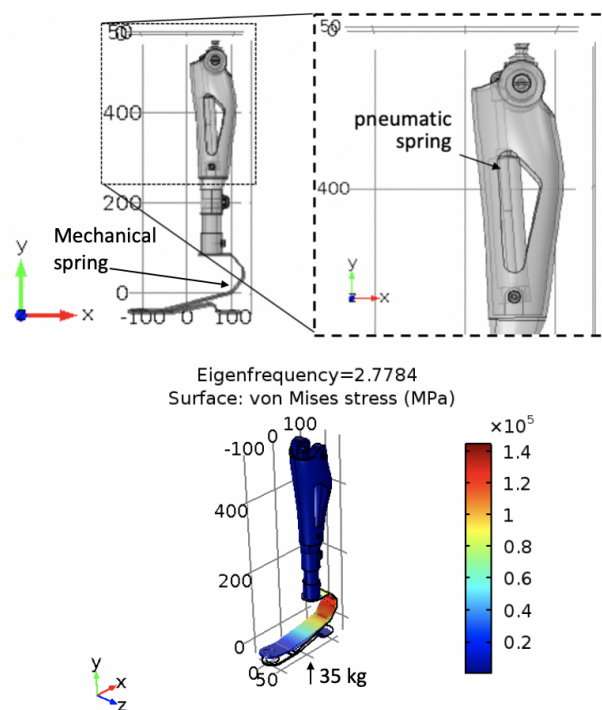


Figure 3. CAD model (**top**) and FEA simulation of the first eigenfrequency (**bottom**) for a carbon fibre prosthetic limb. Thirty-five kilograms of added mass was assumed on the prosthetics to simulate a human above lower limb body mass of 70 kg. The CAD model is adapted from GRABCAD [36].

The spring model diagram can be simplified and expressed by Figure 4. During gait motion, external reaction force from the ground on the prosthetics is expressed by the periodic external forcing $F(t)$. The resonant frequency of the system would be the compound restoring force terms of both the linear mechanical spring and the nonlinear (second-order polynomial) pneumatic spring.

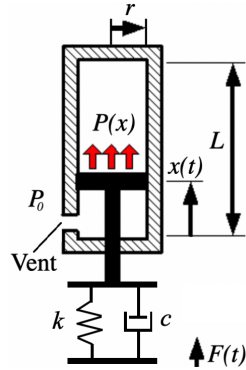


Figure 4. Diagram of pneumatic (air) spring for a simple cylinder, with radius r , length L , displacement $x(t)$, initial (atmospheric) pressure P_0 and gauge pressure $P(x)$, on top of a mechanical spring with stiffness k and damping c . The whole system is subjected to external force $F(t)$, which responds as a spring restoring force $F_s(t)$.

The pneumatic air spring restoring force term is given by Equation (1).

$$F_s(t) = P_0 \pi r^2 \left[\left(\frac{L}{L - x(t)} \right)^\gamma - 1 \right] \quad (1)$$

where F_s is the restoring force of the pneumatic spring mechanism, r is the radius of the pneumatic cylinder radius, L is the pneumatic cylinder length, x is the piston displacement, P_0 is the initial pressure and is equal to 101,325 Pa at the atmospheric pressure, and γ is the diabatic constant that is equal to 1.4 for diatomic gases such as nitrogen and oxygen.

The reason for having this nonlinear second-order spring is to benefit from the nonlinear rapid build up in restoring force as the displacement increases. Therefore, this limits maximum response displacement (thus velocity and acceleration) for typical external forcing beyond a certain amplitude level, which in turn helps to provide comfort to the user. Lower response acceleration implies lower impulse forces experienced during strides.

The amalgamated governing equation of motion for the compound spring system within the prosthetics can thus be described by Equation (2).

$$m\ddot{x} + c\dot{x} + kx + P_0 \pi r^2 \left[\left(\frac{L}{L - x} \right)^\gamma - 1 \right] = F(t) \quad (2)$$

where m is the effective mass of the body load, c is the damping constant, y is the excitation displacement and F is the periodic external response forcing term resulting from the response force from each stride on the ground.

The semi-dimensionless lumped parameter model can be expressed by Equation (3).

$$\ddot{x} + 2\zeta\omega_0\dot{x} + \omega_0^2 x + \frac{P_0}{m} \pi r^2 \left[\left(\frac{L}{L - x} \right)^\gamma - 1 \right] = \ddot{y}(t) \quad (3)$$

where ζ is the dimensionless damping ratio (combining both mechanical and electrical domains), ω_0 is the natural frequency of the mechanical restoring spring system and $\ddot{y}(t)$ is the periodic acceleration input from gait strides.

The total theoretically recoverable power p from the mechanical domain is given by Equation (4), where the mechanical power can be transferred to a hypothetical mechanical-to-electrical transducer.

$$p(t) = -m_t \ddot{y}(t) \dot{y}(t) - m_t \ddot{y}(t) \dot{x}(t) \quad (4)$$

where m_t is the transducer mass.

When the user is running at a stride rate equal to the first resonant frequency, maximum power transfer can be achieved, as represented by Equation (5).

$$p(t) = \frac{m_t \zeta_e \omega_0^3 x(t)^2}{4(\zeta_m + \zeta_e)} \quad (5)$$

where ζ_m and ζ_e are the mechanical and electrical damping ratios, respectively.

However, in practice, only a small fraction of this maximum theoretically recoverable power can actually be converted into useful electrical power [38]. This is due to transducer efficiency, electrical losses and intentional switching design to not extract excessive energy in order not to burden the user with parasitic draining effects.

3.2. Measured Gait Three-Axis Acceleration Data

Figures 5–7 show selected processed and analysis plots for the acceleration data in both time and frequency domains when walking at 3 km/h, running at 9 km/h and walking with 20 kg weight in the right hand, respectively. Please see the Supplementary Materials for more analysis plots of all the various gait conditions. All vibration traces are corrected for 1 gravity offset before applying FFT. Zoomed time windows are shown, illustrating the vibration features during strides.

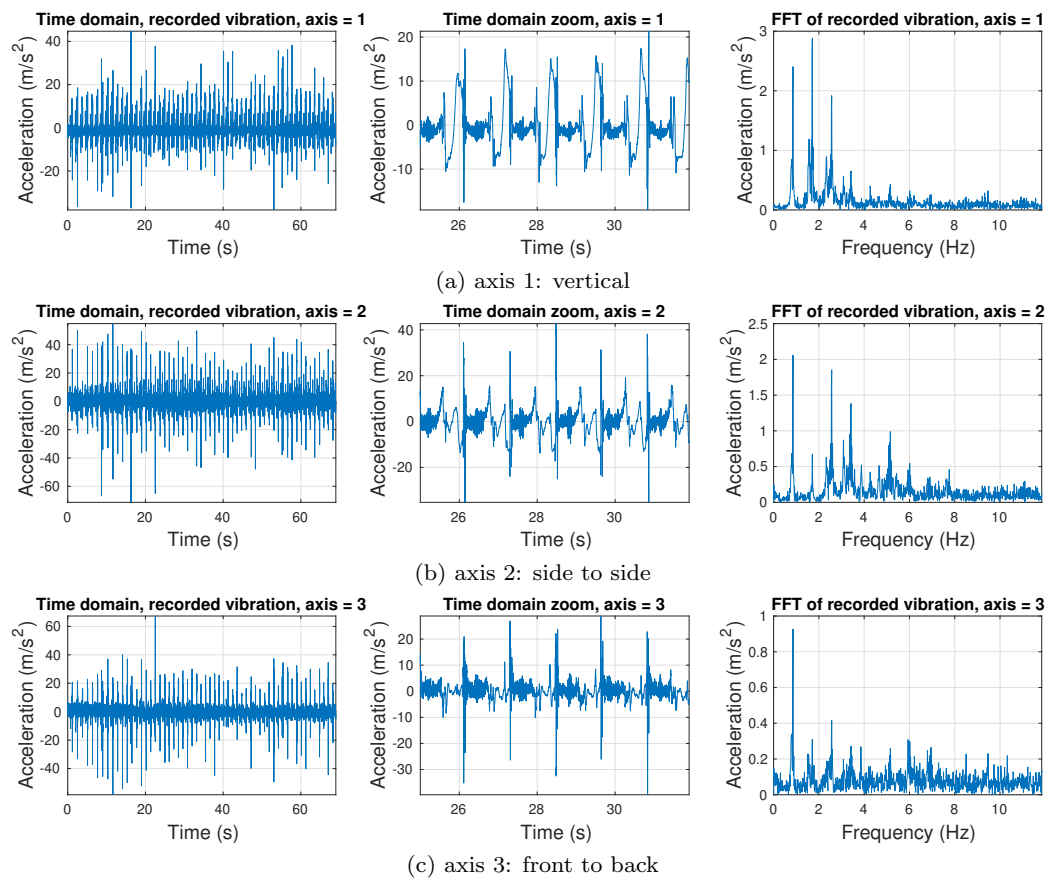


Figure 5. Analysis of gait acceleration in all three axes while walking at 3 km/h.

It can be seen that the acceleration peaks for running gait in Figure 6 are higher than those of the walking gait in Figure 5 for all three axes. Furthermore, the first active frequency peak for walking gait averages at around 0.9 Hz while that for the running gait is at 1.4 Hz. There are clear presence of harmonics in the frequency domain, suggesting some flatness to the peak features during the strides. None of the axes appear to be particularly dominant and all demonstrate relatively substantial amount of kinetic energy. This suggests that energy harvesting will need to be responsive to all three axes in order to be effective in recovering maximum available kinetic energy.

While the pedometric characteristics of the walking and running look qualitatively similar, especially in the frequency domain, this is rather different for the simulated limping scenario shown in Figure 7. There are less harmonics in the frequency domain and shorter impulses in the time domain. While the walking speed is also at 3 km/h as the case in Figure 5, instantaneous acceleration peak are higher in the lopsided walking case. This might be because that the area under the energy curve might be similar for the given walking speed, but more of the energy is concentrated over a shorter stride impact time. Therefore, this makes the impulse forces larger due to the shorter impulse time. Few harmonics could also be a result of sharper and less flat peaks in the time domain.

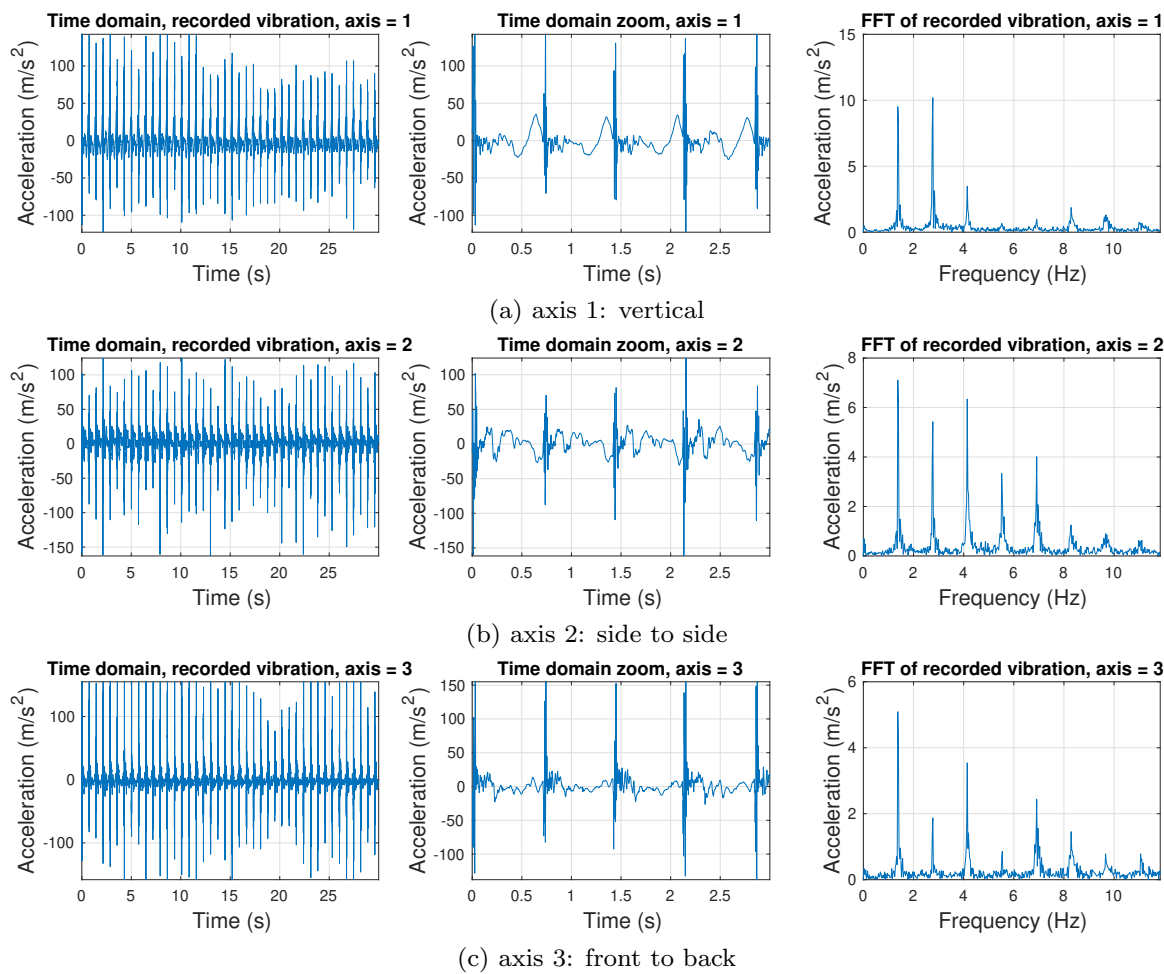


Figure 6. Analysis of gait acceleration in all three axes while running at 9 km/h.

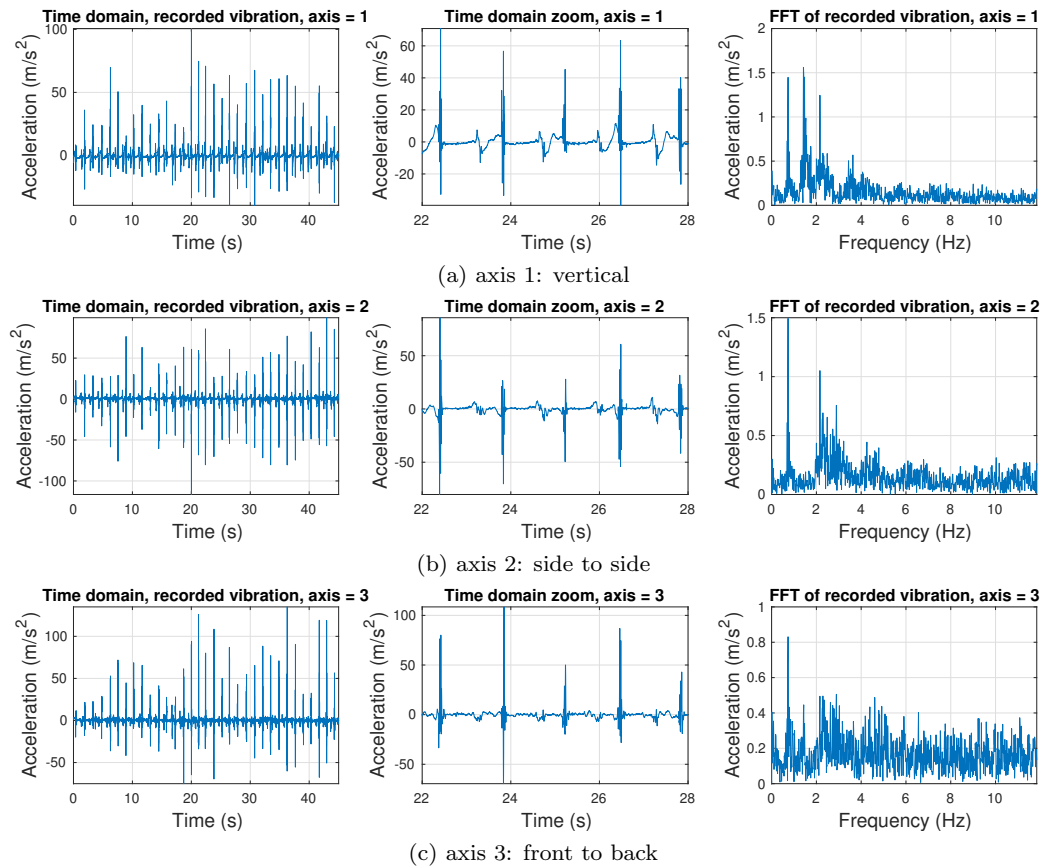


Figure 7. Analysis of gait acceleration in all three axes with 20 kg weight in the right hand to simulate lopsided walking.

3.3. Numerically Simulated Power Prediction

Selected results are shown in Figure 8 and more details results are delineated in Table 1. Only the axis with the maximum power out of the three axes for each gait condition is shown in each respective figure. For most axes, as expected, longitudinal axis generates the highest average power. However, the peak power axis is not necessarily the axis with highest average acceleration. This might suggest a more optimised energy envelope suitable for more efficient energy conversion in a particular axis during certain gait motions. However, this could be the case specific to the particular participant's gait and might vary between various people as gait pattern changes.

Running gait undoubtedly predicted the highest mean power output at 392 mW with a mean input acceleration of 11.3 m/s^2 in the longitudinal axis. However, the 41 mW generated from climbing at 60 steps per minute (3.7 m/s^2) was at a similar level to the 45 mW generated from walking at 3 km/h (4.2 m/s^2). On the other hand, lopsided walking attracted the highest power per acceleration, at 103 mW for just 2.6 m/s^2 average acceleration experienced in the frontal axis (similar levels in the sagittal axis too). However, despite the high peak amplitudes, the time window features are much narrower, suggesting a concentration of energy bursts across a shorter time period.

The energy recovered from simulated limping motion is different between left side and right side. This could be a result of asymmetrical and uneven gait motion of the user. This could be different between various people and gait pattern. Overall, it is unsurprising that running gait generated the most power. However, it can be seen that step climbing gait does not generate much power compared to a walking gait.

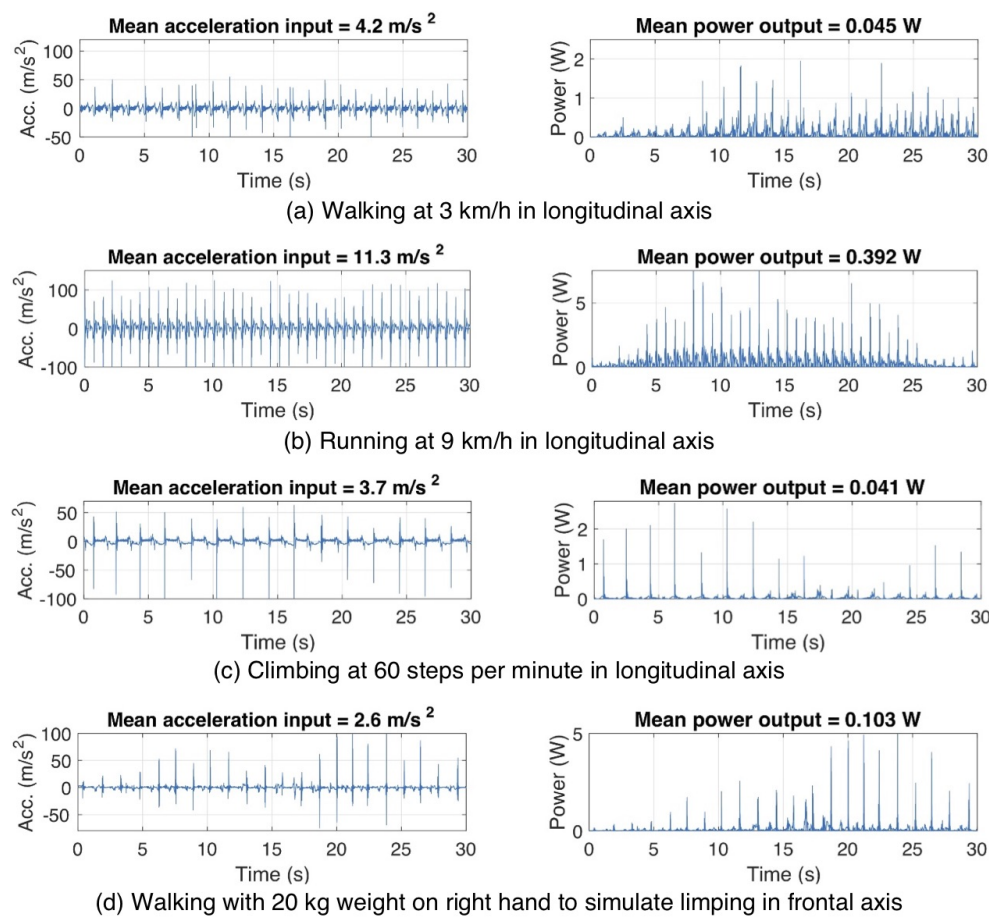


Figure 8. Simulated recoverable power from the prosthetics leg for selected gait conditions and axes.

Table 1. Numerically predicted mean electrical power levels that can be generated from various gait conditions and axes from the regenerative prosthetics (one limb).

Gait Condition	Acc. (m/s ²)	Power (mW)	Axis
Walking at 3 km/h	4.2	31	Sagittal
	4.2	45	Longitudinal
	2.3	34	Frontal
Walking at 6 km/h	7.9	96	Sagittal
	8.1	75	Longitudinal
	6.1	57	Frontal
Running at 9 km/h	11.7	341	Sagittal
	11.3	392	Longitudinal
	9.4	241	Frontal
Climbing at 60 steps per minute	2.3	29	Sagittal
	3.7	41	Longitudinal
	1.9	27	Frontal
Walking with 20 kg weight in the left hand	2.3	87	Sagittal
	2.4	52	Longitudinal
	2.5	62	Frontal
Walking with 20 kg weight in the right hand	2.8	102	Sagittal
	2.7	69	Longitudinal
	2.6	103	Frontal

4. Discussion

To assess the meaningfulness of the recoverable power, the simulated harvestable power values from Table 1 can be compared against the typical power requirement of various sensors, controllers, wireless systems, motors and actuators in Table 2. Energy harvesting itself is impossible to meet the power requirement of the bionic prosthetic as the kinetic energy harnessed is from the gait motion itself. If too much power is harvested, it would start to manifest as a parasitic drain on the user. Therefore, the power recoverable is only meant to supplement the on-board battery and extend operation time between each charge cycles.

Table 2. Typical power requirements P of selected active components in bionics and smart prosthetics.

Device/Operation Mode	P (mW)	Notes
Microprocessing unit (MPU)	0.36	active mode [39]
32-bit ARM Cortex	0.002	standby mode [39]
Bluetooth 5 + RF chip	27 0.045	transceiver mode [40] sleep mode, clock [40]
MEMS 9 DOF motion sensor + MPU	0.05	InvenSense [41]
MEMS strain gauge + ASIC	0.01	Uni. Cambridge [35]
MEMS pressure sensor + ASIC	0.2	Omron [42]
DC Motor at 0.85 kg f.cm torque	4,500	3 units of 1.5 W motor
Servo actuator with 5 N starting force	9,000	3 units of 3 W motor
Power conditioning circuit	0.1	switch mode type [33]
Other electrical components + leakage	0.5	estimate

It can be seen that power recoverable from gait motion is sufficient to meet the power requirements of sensors, microprocessors and wireless systems. Therefore, all sensing and smart computation capabilities can be sustained by regenerative gait energy. The addition of various sensors, including accelerometers, gyroscopes, magnetometers, temperature sensors, pressure sensors, strain gauge and other smart microsensors can help to feedback into the active control loop to enhance motor control for comfort and healthy gait pattern, ensure safety, remind maintenance needs and alert potential system errors. As can be seen, motor and actuator power requirement for active knee and active ankle is more than an order of magnitude than what energy harvesting can provide. Therefore, continuous motor drive is not realistic. However, for practical operations, motors and actuators are not required for continuous operation. Intermittent minute adjustments of knee and ankle angular orientations would be enough to help maintain a comfortable and healthy gait, controlled by the information from the sensor array.

Many of the power consumptions from active components does not need to be in active operation all the time and smart power management coupled with duty-cycling can help to drastically reduce the actual power budget. The most power consuming elements would be the motors and actuators, which can be duty-cycled by adaptive control to help assist adjust gait motion and pattern as required. Wireless communication would be the second most power consuming element, which can also be duty cycled. Table 3 uses the information from Table 2 and assumes a hypothetical case study and estimates a power budget of around 62 mW required by the wireless sensors and motor actuators. This compares favourably with the simulated average power output from Table 1.

A numerical model representing the duty-cycled electrical load combinations from Table 3 was built in MATLAB and integrated with the regenerative prosthetics numerical model. Figures 9 and 10 show the charging and discharging simulation results for two gait patterns: walking and running, respectively. During walking at 6 km/h, the average power output just about meets the average power drain from

the active components, while a running gait is able to generate significantly more power than needed. On the other hand, slow walking and rest periods will incur a dip in the charge reserve in the energy storage. However, apart from trying to match average power consumption by the load, it is also important to ensure that there is sufficient stored energy to draw upon by instantaneous power consumption peaks during active motor and wireless communication operations.

Table 3. Estimated power budget of a hypothetical smart prosthetic bionic leg with wireless sensing functionality and intermittent motor controlled ankle and knee adjustments for gait comfort optimisation.

Power Budget Item	Active Power (W)	Period (s)	Active in Period (%)	Active Time in 1 min. (s)	Average Power in 1 min. (W)
MPU, $\times 4$ units	2.00×10^{-3}	1.0	100	60	2.000×10^{-3}
Bluetooth 5.0 + RF chip Tx, $\times 4$ units	1.08×10^{-1}	5.0	20	12	2.160×10^{-2}
Bluetooth 5.0 + RF chip sleep, $\times 4$ units	1.80×10^{-4}	5.0	80	48	1.440×10^{-4}
MEMS 9 DOF, $\times 4$ units	2.00×10^{-3}	1.0	100	60	2.000×10^{-3}
MEMS pressure sensor, $\times 4$ units	2.00×10^{-3}	1.0	100	60	2.000×10^{-3}
Memory + misc. electric, $\times 4$ units	2.00×10^{-3}	1.0	100	60	2.000×10^{-3}
Power conditioning circuit, $\times 4$ units	4.00×10^{-4}	1.0	100	60	4.000×10^{-4}
Misc. elec. and leakage, $\times 4$ units	2.00×10^{-3}	1.0	100	60	2.000×10^{-3}
DC motor, $\times 3$ units, right ankle	$1.50 \times 10^{+0}$	6.0	0.17	0.1	2.501×10^{-3}
DC motor, $\times 3$ units, left ankle	$1.50 \times 10^{+0}$	6.0	0.17	0.1	2.501×10^{-3}
DC motor, $\times 3$ units, right knee	$1.50 \times 10^{+0}$	6.0	0.17	0.1	2.501×10^{-3}
DC motor, $\times 3$ units, left knee	$1.50 \times 10^{+0}$	6.0	0.17	0.1	2.501×10^{-3}
Servo actuator, $\times 3$ units, right ankle	$3.00 \times 10^{+0}$	6.0	0.17	0.1	5.001×10^{-3}
Servo actuator, $\times 3$ units, left ankle	$3.00 \times 10^{+0}$	6.0	0.17	0.1	5.001×10^{-3}
Servo actuator, $\times 3$ units, right knee	$3.00 \times 10^{+0}$	6.0	0.17	0.1	5.001×10^{-3}
Servo actuator, $\times 3$ units, left knee	$3.00 \times 10^{+0}$	6.0	0.17	0.1	5.001×10^{-3}
Sum					6.215×10^{-2}

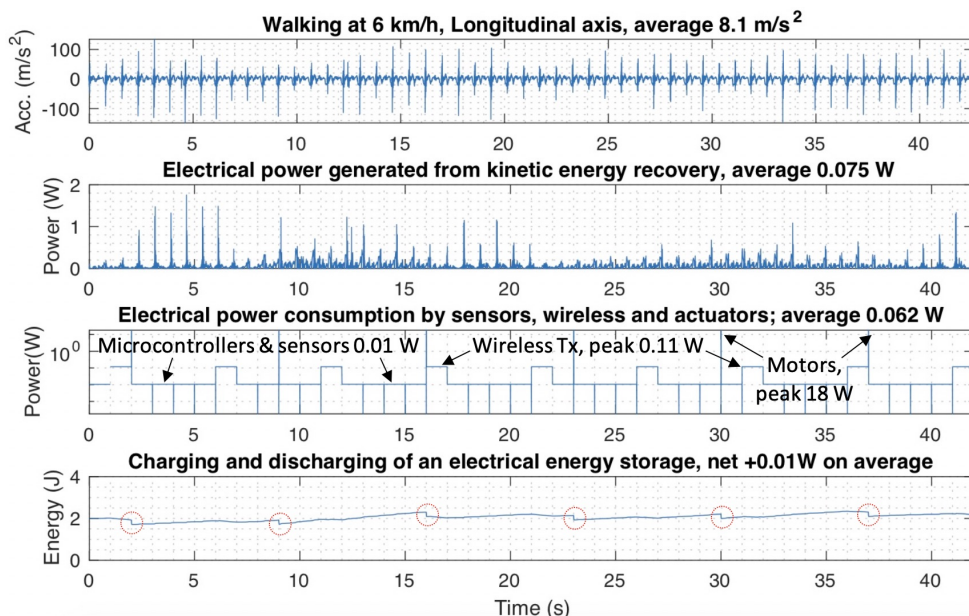


Figure 9. Simulated charging and discharging of an energy storage by energy recovery and electrical load, respectively, for a walking scenario. A starting energy of 2 J is given within the storage.

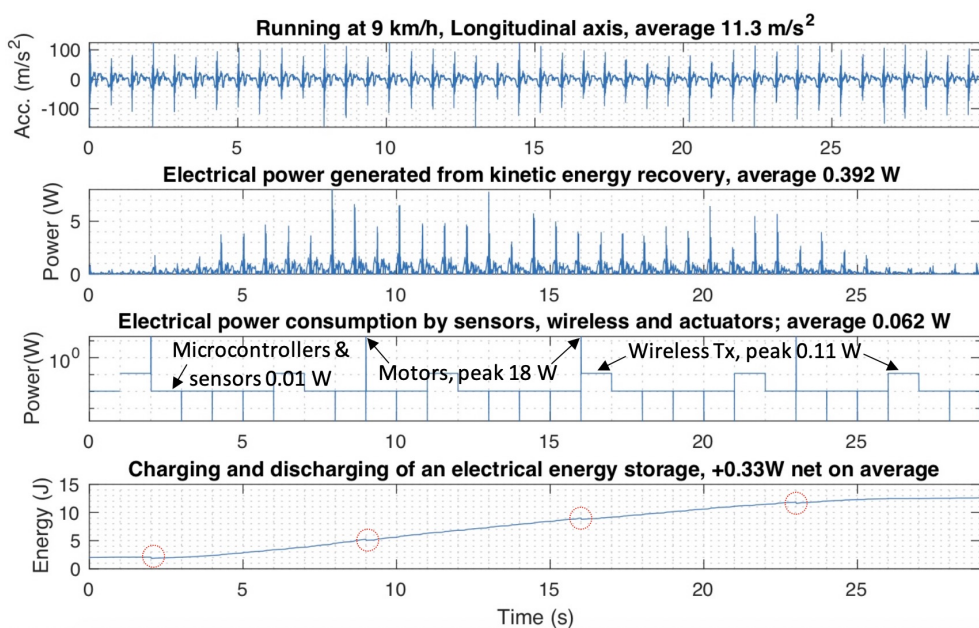


Figure 10. Simulated charging and discharging of an energy storage by energy recovery and electrical load, respectively, for a running scenario. A starting energy of 2 J is given within the storage.

Active motor operations here are assumed to last for 10 ms every 6 s, adjusting ankle and knee orientations to maintain optimal gait. This results in a sharp but short-lived power drain on the energy storage. To buffer for the high instantaneous drain, a minimal threshold charge needs to be maintained in the energy storage. To be practical, on-board batteries should be minimal in size and weight in order to not overburden the user: transtibial amputees. The battery itself can be recharged in a charging hub while the user sleeps in night time, and can be trickle charged by the energy recovered through regenerative gait motion. The presence of regenerative gait can therefore help to minimise the size and weight of on-board battery.

5. Conclusions

This study measured three-axis gait acceleration data from various gait patterns and used the measured data to numerically simulate (MATLAB) a prosthetic leg model containing a pneumatic and mechanical spring. Finite element model (COMSOL) was simulated to inform the system parameters used in the MATLAB numerical model. It is predicted that nearly 0.4 W of average electrical power can be recovered for a running gait (9 km/h) and 45 mW for walking gait (3 km/h). This power level is sufficient to continuously sustain smart microsystems including wireless systems, microprocessing units and MEMS sensors. Furthermore, the power consumed by duty-cycled motors and actuators for driving active bionic knee and ankle (a hypothetical 62 mW average power budget was estimated here) to maintain healthy gait can also be either partially or entirely compensated by energy harvesting in order to make meaningful contributions to extending the battery life.

The results presented here set the scene for developing towards regenerative prosthetics to help sustain the power requirement for smart functionalities (sensors) and supplement the battery drain by bionics (motors). As more sensors and motors are added to develop the comfort and gait pattern of prosthetics, the proposed regenerative energy harvesting capability is crucial to enable these functions without having to overburden the user with a heavy battery pack. Future work is planned by the authors to develop proof-of-concept prototypes on regenerative smart composite lower limb prosthetics.

Author Contributions: Conceptualization, Y.J. and Y.S.; Data curation, Y.S.; Formal analysis, Y.J. and Y.S.; Investigation, Y.J., Y.S. and X.W.; Methodology, Y.J., Y.S. and X.W.; Supervision, Y.J., Y.S., X.W., C.W., P.L. and S.X.; Validation, Y.J., Y.S., J.P., P.X. and T.W.; Visualization, Y.J. and Y.S.; Writing—original draft, Y.J.; Writing—review and editing, Y.J., X.W., J.P., P.X., T.W., C.W., P.L., S.X. and Y.S.

Funding: This research did not receive external funding.

Acknowledgments: This work was supported by internal resources from the Chester Smart Composite Group led by Yu Shi.

Conflicts of Interest: The authors declare no conflict of interest.

Abbreviations

The following abbreviations are used in this manuscript:

ESR	energy storage and return
SACH	solid ankle, cushioned heel
MEMS	microelectromechanical systems
CFRP	carbon fibre reinforced polymer
DOF	degrees of freedom

References

1. Samuelsson, K.A.; Töytäri, O.; Salminen, A.L.; Brandt, Å. Effects of lower limb prosthesis on activity, participation, and quality of life: A systematic review. *Prosthetics Orthot. Int.* **2012**, *36*, 145–158. [[CrossRef](#)]
2. Bliquez, L.J. Classical Prosthetics. *Archaeology* **1983**, *36*, 25–29.
3. Staros, A. The SACH (solid-ankle cushion-heel) foot. *Orthop. Prosthet. Appl. J.* **1957**, *2*, 23–31.
4. Lehmann, J.; Price, R.; Boswell-Bessette, S.; Dralle, A.; Questad, K.; deLateur, B. Comprehensive analysis of energy storing prosthetic feet: Flex Foot and Seattle Foot Versus Standard SACH foot. *Arch. Phys. Med. Rehabil.* **1993**, *74*, 1225–1231. [[CrossRef](#)]
5. Nolan, L. Carbon fibre prostheses and running in amputees: A review. *Foot Ankle Surg.* **2008**, *14*, 125–129. [[CrossRef](#)] [[PubMed](#)]
6. South, B.J.; Fey, N.P.; Bosker, G.; Neptune, R.R. Manufacture of Energy Storage and Return Prosthetic Feet Using Selective Laser Sintering. *J. Biomech. Eng.* **2009**, *132*, 015001. [[CrossRef](#)] [[PubMed](#)]
7. Versluys, R.; Desomer, A.; Lenaerts, G.; Beyl, P.; Van Damme, M.; Vanderborght, B.; Vanderniepen, I.; Van der Perre, G.; Lefebvre, D. From conventional prosthetic feet to bionic feet: A review study. In Proceedings of the 2008 2nd IEEE RAS & EMBS International Conference on Biomedical Robotics and Biomechatronics, Scottsdale, AZ, USA, 19–22 October 2008; pp. 49–54.
8. Versluys, R.; Beyl, P.; Damme, M.V.; Desomer, A.; Ham, R.V.; Lefebvre, D. Prosthetic feet: State-of-the-art review and the importance of mimicking human ankle–foot biomechanics. *Disabil. Rehabil. Assist. Technol.* **2009**, *4*, 65–75. [[CrossRef](#)]
9. Pailler, D.; Sautreuil, P.; Piera, J.; Genty, M.; Goujon, H. Evolution in prostheses for sprinters with lower-limb amputation. *Ann. Readapt. Med. Phys.* **2004**, *47*, 374–381. [[CrossRef](#)] [[PubMed](#)]
10. Scholz, M.S.; Blanchfield, J.; Bloom, L.; Coburn, B.; Elkington, M.; Fuller, J.; Gilbert, M.; Muflahi, S.; Pernice, M.; Rae, S.; et al. The use of composite materials in modern orthopaedic medicine and prosthetic devices: A review. *Compos. Sci. Technol.* **2011**, *71*, 1791–1803. [[CrossRef](#)]
11. Highsmith, M.J.; Kahle, J.T.; Bongiorni, D.R.; Sutton, B.S.; Groer, S.; Kaufman, K.R. Safety, energy efficiency, and cost efficacy of the C-Leg for transfemoral amputees: A review of the literature. *Prosthetics Orthot. Int.* **2010**, *34*, 362–377. [[CrossRef](#)] [[PubMed](#)]
12. Alsaadi, A.; Shi, Y.; Pan, L.; Tao, J.; Jia, Y. Vibration energy harvesting of multifunctional carbon fibre composite laminate structures. *Compos. Sci. Technol.* **2019**, *178*, 1–10. [[CrossRef](#)]
13. Liu, M.; Datseris, P.; Huang, H.H. A Prototype for Smart Prosthetic Legs—Analysis and Mechanical Design. *Adv. Mater. Res.* **2012**, *403–408*, 1999–2006. [[CrossRef](#)]

14. Park, J.; Yoon, G.H.; Kang, J.W.; Choi, S.B. Design and control of a prosthetic leg for above-knee amputees operated in semi-active and active modes. *Smart Mater. Struct.* **2016**, *25*, 085009. [[CrossRef](#)]
15. Sup, F.; Varol, H.A.; Mitchell, J.; Withrow, T.J.; Goldfarb, M. Self-contained powered knee and ankle prosthesis: Initial evaluation on a transfemoral amputee. In Proceedings of the IEEE International Conference on Rehabilitation Robotics, Kyoto, Japan, 23–26 June 2009.
16. Ferreira, C.; Reis, L.P.; Santos, C.P. Review of Control Strategies for Lower Limb Prostheses. In *Robot 2015: Second Iberian Robotics Conference*; Reis, L.P., Moreira, A.P., Lima, P.U., Montano, L., Muñoz-Martinez, V., Eds.; Springer International Publishing: Cham, Switzerland, 2016; pp. 209–220.
17. Windrich, M.; Grimmer, M.; Christ, O.; Rinderknecht, S.; Beckerle, P. Active lower limb prosthetics: A systematic review of design issues and solutions. *Biomed. Eng. Online* **2016**, *15*, 140. [[CrossRef](#)] [[PubMed](#)]
18. Sup, F.; Varol, H.A.; Mitchell, J.; Withrow, T.; Goldfarb, M. Design and control of an active electrical knee and ankle prosthesis. In Proceedings of the 2nd IEEE RAS and EMBS International Conference on Biomedical Robotics and Biomechatronics, Scottsdale, AZ, USA, 19–22 October 2008.
19. Pillai, M.V.; Kazerooni, H.; Hurwich, A. Design of a semi-active knee-ankle prosthesis. In Proceedings of the IEEE International Conference on Robotics and Automation, Shanghai, China, 9–13 May 2011.
20. Tucker, M.R.; Fite, K.B. Mechanical damping with electrical regeneration for a powered transfemoral prosthesis. In Proceedings of the 2010 IEEE/ASME International Conference on Advanced Intelligent Mechatronics, Montreal, ON, Canada, 6–9 July 2010; pp. 13–18.
21. Jia, Y.; Yan, J.; Soga, K.; Seshia, A. A parametrically excited vibration energy harvester. *J. Intel. Mater. Syst. Struct.* **2013**. [[CrossRef](#)]
22. Jia, Y.; Yan, J.; Soga, K.; Seshia, A. Parametric resonance for vibration energy harvesting with design techniques to passively reduce the initiation threshold amplitude. *Smart Mater. Struct.* **2014**, *23*, 13. [[CrossRef](#)]
23. Jia, Y.; Seshia, A. Directly and parametrically excited bi-stable vibration energy harvester for broadband operation. *Proc. Transducers* **2013**, *2013*, 454–457.
24. Jia, Y.; Seshia, A.A. Power Optimization by Mass Tuning for MEMS Piezoelectric Cantilever Vibration Energy Harvesting. *J. MEMS* **2015**, *25*, 108–117. [[CrossRef](#)]
25. Jia, Y.; Yan, J.; Soga, K.; Seshia, A. Parametrically excited MEMS vibration energy harvesters with design approaches to overcome initiation threshold amplitude. *J. Micromech. Microeng.* **2013**, *23*, 10. [[CrossRef](#)]
26. Jia, Y.; Yan, J.; Soga, K.; Seshia, A. Multi-frequency Operation of a MEMS Vibration Energy Harvester by Accessing Five Orders of Parametric Resonance. *J. Phys. Conf. Ser.* **2013**, *476*, 607–611. [[CrossRef](#)]
27. Wang, Z.L. Triboelectric Nanogenerators as New Energy Technology for Self-Powered Systems and as Active Mechanical and Chemical Sensors. *ACS Nano* **2013**, *7*, 9533–9557. [[CrossRef](#)] [[PubMed](#)]
28. Wang, Z.L.; Lin, L.; Chen, J.; Niu, S.; Zi, Y. *Triboelectric Nanogenerators*; Springer: New York, NY, USA, 2016.
29. Priya, S.; Inman, D. *Energy Harvesting Technologies*; Springer: New York, NY, USA, 2009.
30. Gonzalez, J.; Rubio, A.; Moll, F. Human powered piezoelectric batteries to supply power to wearable electronic devices. *Int. J. Soc. Mater. Eng. Resour.* **2002**, *10*, 34–40. [[CrossRef](#)]
31. Mitcheson, P.; Yeatman, E.; Rao, G.; Holmes, A.; Green, T. Energy harvesting from human and machine motion for wireless electronic devices. *Proc. IEEE* **2008**, *96*, 1457–1486. [[CrossRef](#)]
32. Selles, R.W.; Bussmann, J.B.; Wagenaar, R.C.; Stam, H.J. Effects of prosthetic mass and mass distribution on kinematics and energetics of prosthetic gait: A systematic review. *Arch. Phys. Med. Rehabil.* **1999**, *80*, 1593–1599. [[CrossRef](#)]
33. Du, S.; Jia, Y.; Zhao, C.; Amaratunga, G.A.J.; Seshia, A.A. A Fully Integrated Split-Electrode SSHC Rectifier for Piezoelectric Energy Harvesting. *IEEE J.-Solid-State Circuits* **2019**, *54*, 1733–1743. [[CrossRef](#)]
34. Beeby, S.; Tudor, M.; White, N. Energy harvesting vibration sources for microsystems applications. *Meas. Sci. Technol.* **2006**, *17*, R175–R195. [[CrossRef](#)]
35. Jia, Y.; Do, C.D.; Zou, X.; Seshia, A.A. A Hybrid Vibration Powered Microelectromechanical Strain Gauge. *IEEE Sens. J.* **2015**, *16*, 235–241. [[CrossRef](#)]
36. Nox, P. *Prosthetic Leg*; GRABCAD: Cambridge, MA, USA, 2017.

37. AV, R.; MR, S.; RG, E. Influence of speed and step frequency during walking and running on motion sensor output. *Med. Sci. Sport. Exerc.* **2007**, *39*, 716–727.
38. Jia, Y.; Li, S.; Shi, Y. An Analytical and Numerical Study of Magnetic Spring Suspension with Energy Recovery Capabilities. *Energies* **2018**, *11*, 3126. [[CrossRef](#)]
39. STMicroelectronics. *STM32L4 Power Control*; STMicroelectronics: Geneva, Switzerland, 2019.
40. Darroudi, S.M.; Caldera-Sánchez, R.; Gomez, C. Bluetooth Mesh Energy Consumption: A Model. *Sensors* **2019**, *19*, 1238. [[CrossRef](#)]
41. InvenSense. *MPU-9250 Nine-Axis (Gyro + Accelerometer + Compass) MEMS MotionTracking Device*; InvenSense: San Jose, CA, USA, 2019.
42. Omron. *OMRON MEMS Gauge Pressure Sensor 2SMPP-02*; Omron: Kyoto, Japan, 2019.



© 2019 by the authors. Licensee MDPI, Basel, Switzerland. This article is an open access article distributed under the terms and conditions of the Creative Commons Attribution (CC BY) license (<http://creativecommons.org/licenses/by/4.0/>).